IOP Publishing Journal of Optics
J. Opt. **16** (2014) 045004 (9pp) doi:10.1088/2040-8978/16/4/045004

Enhanced transmission via evanescent-to-propagating conversion in metallic nanoslits: role of Rayleigh anomalies

Diana C Skigin[1,2] **and Marcelo Lester**[3,4]

[1] Grupo de Electromagnetismo Aplicado, Departamento de Física, Facultad de Ciencias Exactas y Naturales, Universidad de Buenos Aires, Ciudad Universitaria, Pabellón I, C1428EHA Buenos Aires, Argentina
[2] IFIBA-CONICET, Argentina
[3] Grupo de Óptica de Sólidos-Elfo, Centro de Investigaciones en Física e Ingeniería del Centro de la Provincia de Buenos Aires, Argentina
[4] Instituto de Física Arroyo Seco, Facultad de Ciencias Exactas, Universidad Nacional del Centro de la Provincia de Buenos Aires, Pinto 399, 7000 Buenos Aires, Argentina

E-mail: dcs@df.uba.ar and mlester@exa.unicen.edu.ar

Received 8 January 2014, revised 24 February 2014
Accepted for publication 25 February 2014
Published 19 March 2014

Abstract

We analyze the enhanced transmission phenomenon in subwavelength slit structures near a dielectric interface. In particular, we investigate the influence of Rayleigh anomalies in the spectral position as well as in the bandwidth of Fabry–Perot resonances excited on such structures. We consider the cases of propagating and evanescent incidence, i.e., when the metallic structure is illuminated from the dielectric medium side with an incidence angle larger than the critical angle. We show that Rayleigh anomalies strongly interact with Fabry–Perot resonances, and make them deviate from the spectral positions predicted by the infinitely thin slit model. To get physical insight into this problem, we develop a simplified electromagnetic model and show that there is a close correspondence between the transmitted response of the structure and the behavior of certain function that depends on the geometrical and the illumination parameters. Our results suggest that Rayleigh anomalies strongly modify the electromagnetic response of the structure due to the existence of surface waves that modify the coupling condition between the fields inside and outside the slits. Besides, we show that even in absence of Fabry–Perot resonances, it is possible to produce enhanced transmission by taking advantage of the pseudoperiodicity condition of the fields.

Keywords: enhanced transmission, nanostructures, subwavelength slits
PACS numbers: 42.25.Fx, 42.79.Dj

(Some figures may appear in colour only in the online journal)

1. Introduction

The study of evanescent-to-propagating waves conversion mechanisms by means of diffractive devices with subwavelength features has attracted increasing interest in the last few years. The goal of these studies is focused on exploring the possibility of generating optical images with details much smaller than the limit size imposed by the diffraction limit. The common physical principle underlying the design of these devices is to increase the spectrum of the momentum associated with the electromagnetic wave (Δk) so that smaller details can be imaged ($\Delta k \Delta x \approx 2\pi$). This simple relationship,

which accounts for the balance between momentum and localization, has permitted the development of near field superlenses and hyperlenses [1]. Such devices convert evanescent into propagating waves and can achieve resolutions below $\lambda/5$ [2, 3].

Recently, the combined effect produced by different resonant mechanisms on the transmitted response of metallic slit gratings, such as Fabry–Perot resonances, surface plasmon excitation and Wood–Rayleigh anomalies, has been investigated [4–7]. However, only a few works deal with the problem of enhanced transmission by subwavelength slits under evanescent incidence. In [8, 9] the authors investigate the scattering by an opaque screen with a single slit illuminated by evanescent waves generated at a prism under total internal reflection (TIR). In previous works we have reported the possibility of evanescent-to-propagating conversion by means of a periodic array of wires near a dielectric interface at which evanescent waves are generated. We have shown that by taking advantage of the pseudoperiodicity property of the electromagnetic field, the transmitted intensity can be increased by means of shape resonances (s-polarization) [10] and of the excitation of eigenmodes within the gap between the array and the interface (p-polarization) [11].

On the other hand, it was found that the physical mechanism responsible for enhanced transmission by a periodic array of subwavelength slits (a diffraction grating with a large filling factor), is intimately related to the excitation of FP resonances [12]. As a consequence, an appropriate combination of both features, i.e., evanescent waves and subwavelength slits, might produce efficient evanescent-to-propagating conversion, that could be further intensified by the enhanced transmission mechanism.

In this paper we explore this mechanism and investigate the enhanced transmission phenomenon produced by a periodic array of perfectly conducting wires near a dielectric interface, where it is possible to generate both propagating and evanescent waves. In section 2 we introduce the system under study and consider the case of a propagating wave incident on the wire array. We analyze the transmitted response in terms of FP resonances and study the influence of Rayleigh anomalies (RAs). In section 3 we investigate the case of an evanescent wave impinging on the structure, and compare the results with those corresponding to the propagating case. An analysis of the underlying physical mechanisms is done in section 4, where we develop a simplified model to predict the spectral position of the resonances, for both types of incident waves. The near field patterns at particular resonant and non-resonant situations are shown and analyzed in section 5. Finally, concluding remarks are given in section 6.

2. Enhanced transmission by subwavelength slits: propagating incidence

The enhanced transmission phenomenon has prompted many studies intended to deeply understand the physical mechanisms involved. In this section we review and summarize these mechanisms, in the particular case of subwavelength slits in a perfectly conducting screen under propagating incidence.

We consider a periodic structure comprising perfectly conducting wires and subwavelength slits near a dielectric interface, as shown in figure 1. The structure is illuminated from the upper medium (ϵ_1) by a p-polarized plane wave of wavelength λ forming an angle θ_0 with the y axis. The period of the structure is d, the wires' thickness is h and the slits width is c. The array is separated by a distance e from the interface between region 1 (ϵ_1) and region 2 (ϵ_0). To solve the diffraction problem we apply the modal method [10].

One of the more successful models used to explain enhanced transmission by subwavelength slits is the excitation of FP resonances [13, 14]. If the slits are periodically distributed, the pseudoperiodicity condition of the fields strongly affects the electromagnetic response by different mechanisms such as RAs, surface plasmons, or other surface waves. For the particular case of a perfectly conducting structure, the only mechanism responsible for the enhanced transmission is the FP resonance excitation, and the only set of anomalies that influence the transmitted far field are the RAs, which take place when a diffraction order becomes grazing. The RA condition for the transmitted orders is:

$$\sin(\theta_0) = \left(\pm 1 - n\,\frac{\lambda}{d}\right)\frac{1}{\sqrt{\epsilon_1}} \qquad \text{with } n \in Z, \qquad (1)$$

and for the reflected orders:

$$\sin(\theta_0) = \left(\pm 1 - n\,\frac{1}{\sqrt{\epsilon_1}}\,\frac{\lambda}{d}\right) \qquad \text{with } n \in Z, \qquad (2)$$

where n denotes the diffraction order. Rayleigh anomalies manifest themselves as abrupt changes in the electromagnetic field amplitudes due to the power rearrangement that takes place when a diffraction order appears or disappears. In general, under a RA condition, transmission minima are observed. These anomalies strongly interact with FP resonances. A similar phenomenon has been experimentally observed, in which FP resonances interact with Wood anomalies for propagating waves [15]. Actually, Rayleigh and Wood anomalies describe qualitatively similar and very close curves in the $\theta_0 - \lambda$ plane, which are difficult to separate from each other.

In figure 2 we show a contour plot of the total transmitted efficiency as a function of the incidence angle and of the wavelength-to-period ratio λ/d, for two different values of the normalized depth h/d. The high transmission zones (red) in both panels correspond to FP resonances, which for an infinitely thin slit should be located at $\lambda/d = 2h/m$ (with $m \in Z > 0$), i.e., at $\lambda/d = 2.6$, 1.3, 0.86, etc, for $h/d = 1.3$ (figure 2(a)) and at $\lambda/d = 1.8$, 0.9, 0.6, etc, for $h/d = 0.9$ (figure 2(b)). It can be observed that in both cases the FP resonances are slightly shifted to longer wavelengths (at $\lambda/d \approx 2.8$, 1.4, 1, etc, for figure 2(a) and at $\lambda/d \approx 2$, 1.1, 0.65, etc, for figure 2(b)), as already reported for finite width slits [16, 17]. There are rather wide regions of the $\theta_0 - \lambda/d$ plane at which neither the spectral width of the peaks nor their intensity, depend on the incidence angle. The spectral location of the FP maxima should be, in principle, angle independent, as it results from the application of the effective refraction index model [18, 19], and it should only depend on geometrical

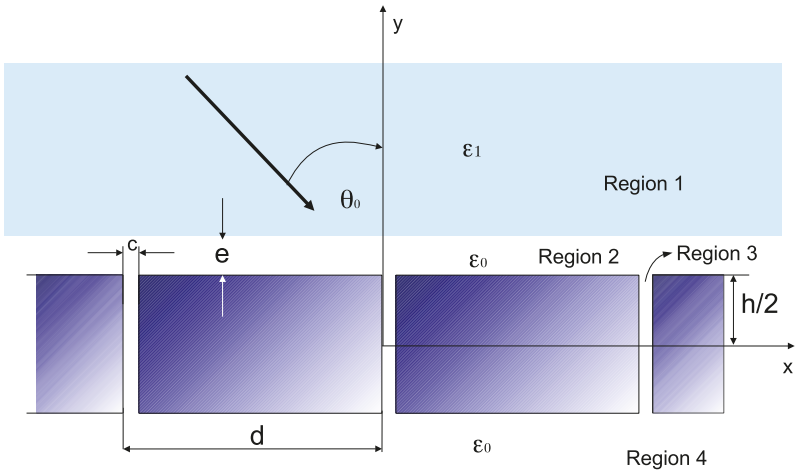

Figure 1. Scheme of the diffraction problem under study. A p-polarized plane wave of wavelength λ impinges with an angle θ_0 on the planar interface between the media with ϵ_1 and ϵ_0. The periodic slit structure is placed at a distance e below the interface.

parameters. This behavior of the FP resonances is verified in figure 2 when FP resonances fall rather far from the RAs. However, the effect of RAs in these figures is remarkable: the spectral location of the FP maxima is strongly distorted by the presence of RAs, which are a consequence of the periodicity condition. It is interesting to notice that for incidence angles $\theta_0 > 55°$, the nature of the FP resonances starts to modify: the resonant peaks widen in such a way that for grazing incidence the overlap between adjacent maxima is very large and the transmission is enhanced for all values of the wavelength.

The existence of RAs implies the presence of evanescent waves that propagate along the surface of the structure. Analogously to surface plasmons, these waves have a complex propagation constant $\alpha = a + ib$. As the incidence angle approaches the condition of appearance of a new diffraction order, $b \to 0$ and a takes a value smaller than 1. The presence of such waves along the structure surface might locally modify the propagation conditions and, as a consequence, could affect the excitation of FP resonances.

To summarize, FP resonances are structure shape resonances and correspond to the excitation of eigenmodes of the slits, which, in turn, are associated to complex poles of the propagation constants of the guided modes along these slits. If local changes are introduced in the coupling conditions (for instance, via the presence of surface waves), the effective refraction index of the slits is modified, and this produces a change in the resonant propagation constant. This behavior is analyzed in section 4.

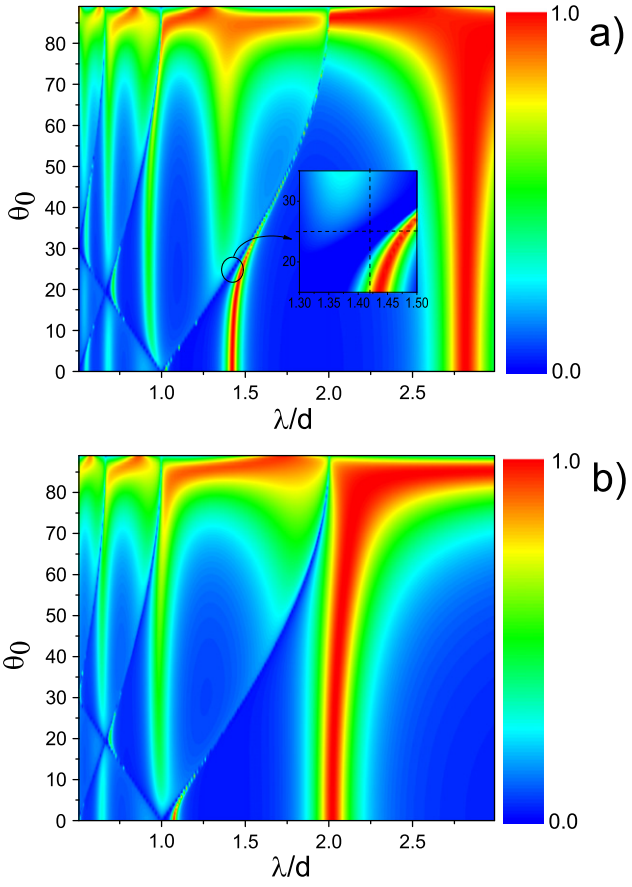

Figure 2. Total transmitted efficiency as a function of λ/d and θ_0, for a perfectly conducting wire grating with $c/d = 0.08$, in the propagating incidence case: $\epsilon_1 = \epsilon_0$. (a) $h/d = 1.3$; (b) $h/d = 0.9$.

3. Enhanced transmission by subwavelength slits: evanescent incidence

In this section we consider a plane wave incident from a medium with dielectric constant $\epsilon_1 > \epsilon_0$. For incidence angles larger than the critical angle, at which the TIR condition is enabled, the pseudoperiodicity condition imposed by the perfect periodicity of the slits array allows transmission to the far field. Unlike the previous case of propagating incidence, we have now a new variable to consider, the distance between the planar dielectric interface and the slits array (e), which would play an important role in the enhanced transmission phenomenon.

In figure 3 we show the contour plot of the total transmitted efficiency for the case in which $\sqrt{\epsilon_1} = 1.5$, $e/d = 0.1$ and

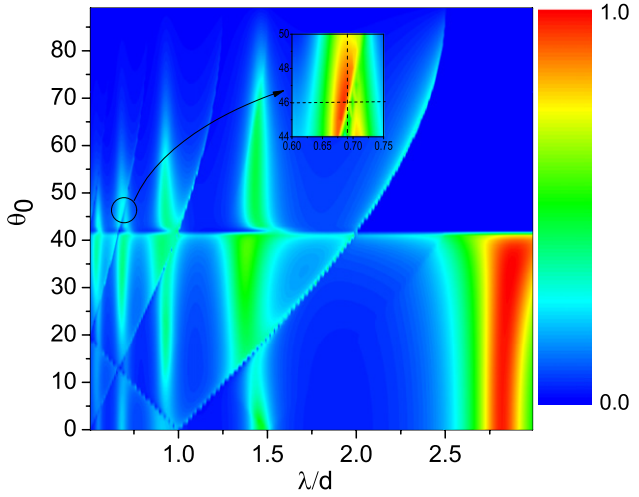

Figure 3. Total transmitted efficiency as a function of λ/d and θ_0 for a perfectly conducting wire grating with $c/d = 0.08$ and $h/d = 1.3$, for $\sqrt{\epsilon_1} = 1.5$ and $e/d = 0.1$.

$h/d = 1.3$. Therefore, the critical angle for this case is $\theta_c \approx 41.8°$. Hence, for $\theta_0 < \theta_c$ we have a propagating wave impinging on the slit structure, whereas for $\theta_0 > \theta_c$ the evanescent waves generated by TIR are responsible for the observed far field transmission. These two regimes are very clearly identified in figure 3.

As in the case of propagating incidence, bands of enhanced transmission associated with FP resonances are observed. Unlike the propagating incidence case, for evanescent incidence ($\theta_0 > \theta_c$) there is a range of incidence angles that maximize the transmittance. According to the grating equation for the transmitted orders, these incidence directions are associated to observation directions of enhanced transmission. This implies that the directionality of the enhancement is governed by both λ/d and θ_0.

As observed, the high transmission bands are strongly affected by the RAs. The spectral location of the enhanced peaks, which carry more than 50% of the diffracted power, are significantly modified in the vicinity of a RA. It can be noticed in figure 3 that the first FP mode, located at $\lambda/d \approx 2.8$, disappears for $\theta_0 > \theta_c$. This occurs since transmission is not allowed for wavelengths close to this resonant wavelength for incidence angles larger than the critical angle. This can be clearly observed as a dark region (blue zone) in the upper right zone of figure 3.

In figure 4 we show contour plots of the -1 transmitted order efficiency as a function of λ/d and θ_0 under an evanescent wave incidence, i.e., for $\theta_0 > \theta_c$. The different panels correspond to different values of the distance e. In figure 4(a) we consider the case in which the array is almost in contact with the planar interface ($e/d = 0.001$). In this figure, solid squares indicate the RAs corresponding to the transmitted orders (given by equation (1)), whereas open circles represent the RAs corresponding to the reflected diffraction orders given by equation (2). In this particular case, the higher enhancement due to FP resonances appears near grazing incidence angles. It can also be observed that the transmission is intensified along the RAs, as it can be noticed, for instance, along the RA that starts at $\lambda/d = 1$ and passes by $\lambda/d = 2$ for $\theta_0 = 42°$. In particular, the first and second FP resonances, take up to 90% of the incident power for almost grazing incidence. RAs also affect the spectral location of these maxima: we have already seen that for these parameters, the second FP resonance occurs at $\lambda/d \approx 1.42$ (figures 2(a) and 3). However, in figure 4(a) we find that at grazing incidence, the maximum enhancement is found for $\lambda/d \approx 1.75$. The third FP mode appears at $\lambda/d \approx 0.94$ and the fourth can hardly be visualized at $\lambda/d \approx 0.71$. All these features suggest that RAs clearly influence the transmission properties of the structure.

The transmitted efficiency map substantially changes when the slit array is moved away from the dielectric interface. In figure 4(b) we consider $e/d = 0.1$, and it can be observed that the FP resonances move to smaller incidence angles, and, contrarily to what occurs in the almost touching case (figure 4(a)), the regions of maximum transmittance cover wide angle bands, and reach at most the 45% of the incident power. Besides, RAs cross the 3rd, 4th and 5th FP resonances, and produce cuts in the zones of enhanced transmission. The trend of the contour plot of figure 4(c), which corresponds to a distance $e/d = 0.2$, is similar to that observed in figure 4(b). However, in figure 4(c) the FP bands are even more constrained in incidence angles, the maximum enhancement is obtained for θ_0 closer to θ_c, and the efficiency rapidly decays as the resonance mode increases. This behavior is even more pronounced for $e/d = 0.3$, as observed in figure 4(d).

It becomes evident that transmission maxima, given by the FP resonances, can be designed to occur in the desired direction: by keeping fixed the geometrical parameters of the periodic structure and varying the distance between the planar interface and the slit array, one could focus these maxima for different incidence angles. Besides, the direction of the transmitted orders vary with the incidence angle. For instance, in the case of figure 4(a) the transmission maxima are found near grazing incidence angles and most of the transmitted power is carried by the -1 order, which propagates almost normally to the structure.

It is to expect that when the thickness of the slit structure is modified, the transmitted efficiency distribution also changes. As stated above, the spectral location of the FP resonances mainly depend on the thickness h of the slits, and this becomes evident in figure 5, where we show contour plots of transmitted efficiency of the -1 order for different values of h/d. However, on top of this well known behavior, in this case the RAs also play a key role. For small values of h/d, i.e., when almost no FP resonances are expected to be excited, the RA appears as an extremely thin band of high transmission. In this case, there is a transmission enhancement of $\approx$33% for $\theta_0 \approx \theta_c$ and for a narrow spectral band. This result is in agreement with those reported in [8] for a single slit in a silver thin film, where the authors found that the incidence angle that maximizes the transmittance is precisely the critical angle. Although in our structure the slits are periodically distributed and then it constitutes a different system from that considered in [8], in this particular case of a small thickness of the metallic screen, the responses of both structures can be compared, and a qualitative agreement is obtained.

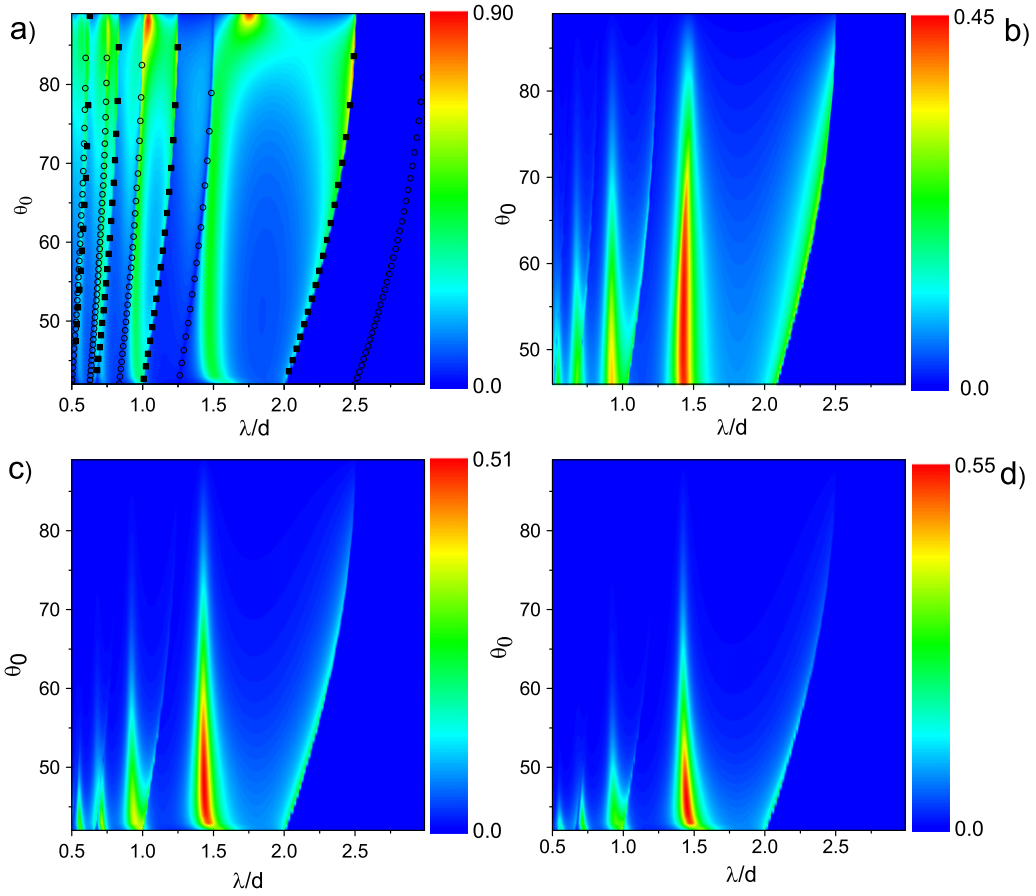

Figure 4. Contour plots of the efficiency of the -1 transmitted order as a function of λ/d and θ_0, for $\sqrt{\epsilon_1} = 1.5$, $h/d = 1.3$, and for $\theta_0 > \theta_c$. Each panel corresponds to a different value of the distance e between the planar interface and the slits array: (a) $e/d = 0.001$; (b) $e/d = 0.1$; (c) $e/d = 0.2$; (d) $e/d = 0.3$. In panel (a) the solid squares indicate the RAs corresponding to the transmitted orders (given by equation (1)) and the open circles represent the RAs corresponding to the reflected diffraction orders given by equation (2).

From the above results corresponding to evanescent wave incidence, it becomes evident that RAs significantly affect the spectral location of the FP resonances, and therefore, the transmission enhancement strongly depends on the angle of incidence and of the distance between the array and the interface. It is interesting to notice that RAs produce evanescent-to-propagating conversion, independently of the FP resonances. It can be observed, for instance, in figure 5(a) along the -1 order anomaly that starts at $\lambda/d = 2$.

4. Simplified model for the prediction of FP resonances

It is well known that simplified and approximate models can help understand the physics involved in the electromagnetic response of complex structures. In particular, several approaches have been proposed for systems comprising metallic wires and slits [12, 14, 20, 21].

According to figure 1, to solve the diffraction problem for the structure under study, the space can be divided into four regions: within the dielectric of ϵ_1 (region 1), between the array and the dielectric interface (region 2), within the slits (region 3), and below the structure (region 4). The modal method consists in expanding the fields in each region in its own eigenfunctions, and then matching them by imposing the boundary conditions at each interface between regions. The results shown in figures 2–5 have been calculated using full modal expansions for the fields within the slits. However, since the structure under study has subwavelength slits, the field within each slit can be approximated by the fundamental mode only, which for p-polarized illumination corresponds to a constant field in the x direction.

Therefore, within this approximation, the complete expression of the magnetic field for p-polarization is:

$$
\begin{aligned}
H_z^{(1)}(x, y) &= \exp\left[\mathrm{i}(\alpha_0 x - \beta_0 (y - y_{\mathrm{int}}))\right] \\
&\quad + \sum_n R_n \exp\left[\mathrm{i}(\alpha_n x + \beta_{1n} (y - y_{\mathrm{int}}))\right], \\
H_z^{(2)}(x, y) &= \sum_n A_n \exp\left[\mathrm{i}(\alpha_n x - \beta_{2n} (y - h/2))\right] \\
&\quad + \sum_n B_n \exp\left[\mathrm{i}(\alpha_n x + \beta_{2n} (y - h/2))\right], \\
H_z^{(3)}(x, y) &= a \cos(ky) + b \sin(ky), \\
H_z^{(4)}(x, y) &= \sum_n T_n \exp\left[\mathrm{i}(\alpha_n x - \beta_{2n} (y + h/2))\right],
\end{aligned}
\tag{3}
$$

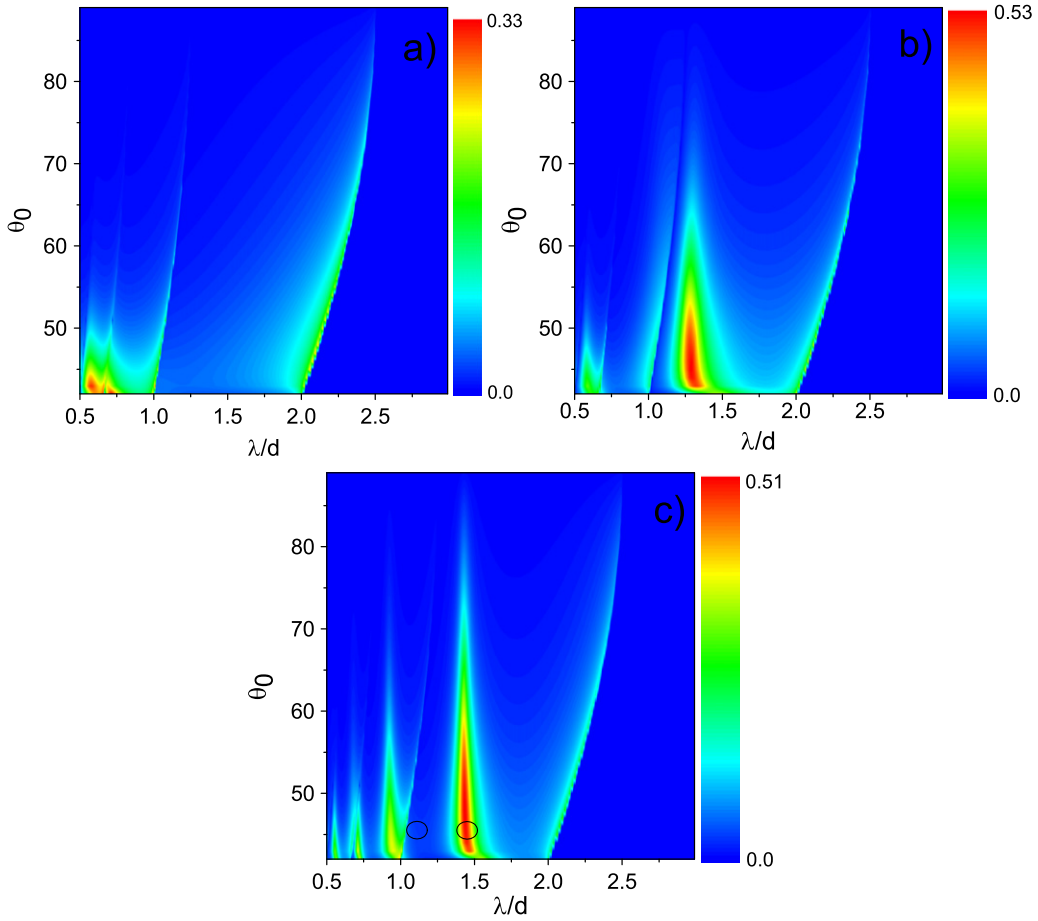

Figure 5. Contour plots of the efficiency of the -1 transmitted order as a function of λ/d and θ_0, for $\sqrt{\epsilon_1} = 1.5$, $e/d = 0.2$, and for $\theta_0 > \theta_c$. Each panel corresponds to a different value of the thickness h of the metallic screen: (a) $h/d = 0.2$; (b) $h/d = 0.5$; (c) $h/d = 1.3$.

where

$$\begin{aligned} \alpha_0 &= \frac{2\pi}{\lambda}\sqrt{\epsilon_1}\sin\theta_0, \\ \alpha_n &= \alpha_0 + n\frac{2\pi}{d}, \\ \beta_{1n}^2 &= \left(\frac{2\pi}{\lambda}\right)^2 \epsilon_1 - \alpha_n^2, \\ \beta_{2n}^2 &= \left(\frac{2\pi}{\lambda}\right)^2 - \alpha_n^2, \end{aligned} \tag{4}$$

$k = \omega/c$ is the propagation constant in vacuum, θ_0 is the angle of incidence, $y_{\text{int}} = h/2 + e$, A_n and B_n are the unknown amplitudes in region 2, a and b are the unknown modal amplitudes, and R_n and T_n are the unknown reflected and transmitted Rayleigh amplitudes, respectively.

By applying the boundary conditions at the interfaces between regions, i.e., at $y = \pm h/2$ and at $y = y_{\text{int}}$, six x-dependent equations are obtained, from which the spatial dependence can be eliminated after appropriate projections. From this set of equations, one can obtain all the unknown amplitudes, and then, the electromagnetic field can be found everywhere. Regarding the problem under study, we are interested in finding an expression for the modal amplitudes that could help us to interpret the physical mechanisms underlying the resonant behavior observed. Then, by conveniently handling these equations, we obtain the following expressions for the modal amplitudes:

$$\begin{aligned} \tilde{a} &= a\cos(kh/2) = \frac{V(SD_1 + c)}{\Delta}, \\ \tilde{b} &= b\sin(kh/2) = \frac{-V(SD_2 - c)}{\Delta}, \end{aligned} \tag{5}$$

where the explicit expressions of Δ, S, V, D_1 and D_2 are given in the appendix. According to the above equations, the denominator Δ plays a key role in the excitation of FP resonances. In what follows, we analyze the behavior of Δ as a function of λ/d and of θ_0 for the structures considered in figures 2(a) and 3, and these results are shown in figure 6 as contour plots of $\text{Re}(\Delta)$ and $\text{Im}(\Delta)$.

As already reported in previous papers [12, 14, 20], the zeros of $\text{Re}(\Delta)$ govern the spectral position of the FP resonances, and $\text{Im}(\Delta)$ accounts for their bandwidth. In figure 6(a) we highlight in black the zeros of $\text{Re}(\Delta)$. By comparing this figure with figure 2(a), it can be observed that the transmission maxima have a clear correlation with the location of the zeros of $\text{Re}(\Delta)$. Notice the strong influence that the RAs produce over the FPs, such that make them deviate from the location predicted according to the infinitely thin slit model. Taking into account that the RA represents a grazing wave, it modifies the coupling conditions and produces a shift in the spectral position of FP resonances, which can be interpreted as a local change of effective refraction index. In

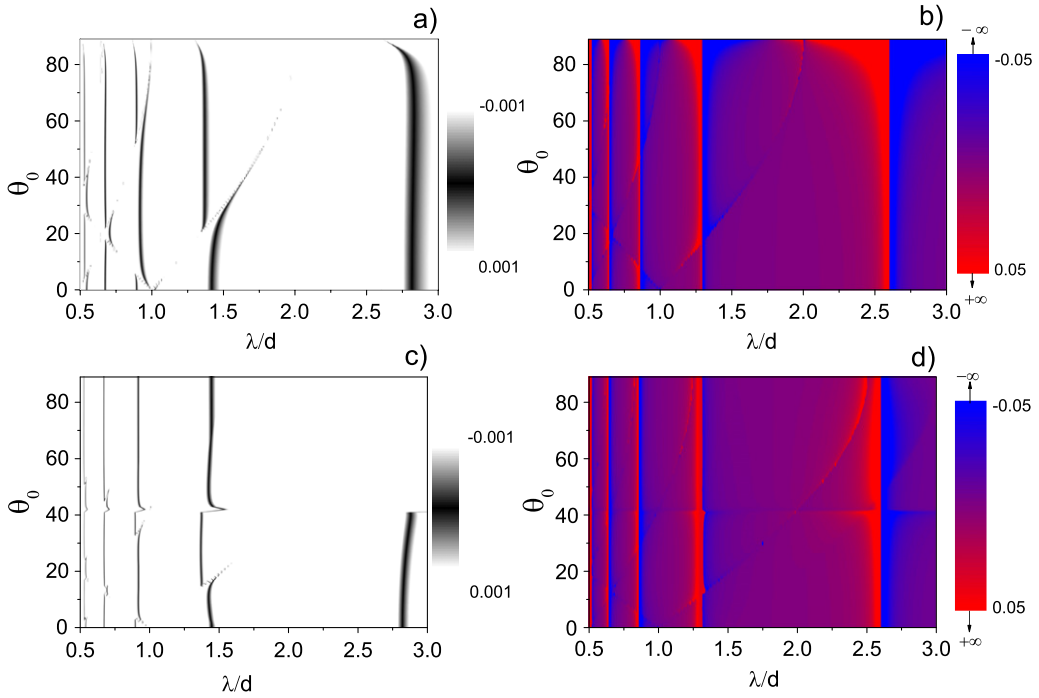

Figure 6. Real and Imaginary parts of Δ, for the structures considered in figures 2(a) and 3. (a) Re(Δ) for the parameters of figure 2(a); (b) Im(Δ) for the parameters of figure 2(a); (c) Re(Δ) for the parameters of figure 3; (d) Im(Δ) for the parameters of figure 3. They gray scale used in panels (a) and (c) highlight the region near zero.

figure 6(b) we show Im(Δ) for this case, where the color scale has been chosen to highlight the relevant characteristics of this function. An increase of |Im(Δ)| can be observed for all wavelengths near grazing incidence angles. This behavior can explain the widening of the enhanced transmission peaks for these incidence angles, as observed in figure 2(a). The asymptotic behavior manifested as vertical lines has already been reported in [14].

In figures 6(c) and (d) we analyze the behavior of Re(Δ) and Im(Δ) for the parameters of figure 3. Notice that the zero of Re(Δ) corresponding to the 1st FP mode disappears for $\theta_0 > \theta_c$. Besides, in the vicinity of the critical angle (≈41.8°), the vertical fringes that correspond to the zeros of Re(Δ) are perturbed. A similar behavior has already been observed near a RA. As in the previous case, the zeros of Re(Δ) are strongly affected by the RAs. The behavior of Im(Δ) in the evanescent incidence case (figure 6(d)) is similar to that observed in the propagating incidence case (figure 6(b)). However, the existence of a critical angle perturbs the spectral position of the FP resonances, as observed for the corresponding Re(Δ). Unlike figure 6(b), in this case the function Im(Δ) is virtually independent of θ_0. This could explain why in this case the transmitted response does not exhibit wide maxima for grazing incidence (see figure 3).

5. Near field

In order to investigate the physical mechanisms that generate the observed far field response of the structure, in this section we show contour plots of near field intensity in several situations of interest. In particular, we analyze the regions at which a RA crosses a FP maximum band, as, for instance, in the circled region of figure 2(a) (propagating incidence) and of figure 3 (evanescent incidence). In figure 7(a) we plot the near field for a structure with $\epsilon_1 = \epsilon_0$, $h/d = 1.3$, $\theta_0 = 25°$ and $\lambda/d = 1.42$, and in figure 7(b) we consider $\sqrt{\epsilon_1} = 1.5$, $h/d = 1.3$, $e/d = 0.1$, $\theta_0 = 46°$ and $\lambda/d = 0.69$.

For the propagating incidence case (figure 7(a)), the transmitted near field is significantly reduced and a propagating wave almost parallel to the structure can be distinguished (lower part). In this case, the RA occurs at $\theta_0 = 24.8°$ for $\lambda/d = 1.42$, and then for $\theta_0 = 25°$ the observed field corresponds to the -1 transmitted order, which propagates along an almost grazing direction. In the upper region, a clear interference pattern is observed, which is formed by the incident and the reflected fields. On the other hand, figure 7(b) illustrates the case of an evanescent wave incidence, which is generated at the dielectric interface indicated by a dashed line, in the upper region. The values of $\theta_0 = 46°$ and $\lambda/d = 0.69$ correspond to the vicinity of the -3rd order RA, which interacts with the 3rd FP mode (see inset in figure 3). The total transmitted field in this case is the superposition of the diffraction orders -1, -2 and -3 (order -3 propagates parallel to the structure).

In figure 8 we show contour plots of the near field intensity corresponding to the pairs θ_0–λ/d circled in figure 5(c), i.e., $\theta_0 = 46°$ and $\lambda/d = 1.45$ (resonant case, figures 8(a) and (b)), and $\theta_0 = 46°$ and $\lambda/d = 1.1$ (non-resonant case, figure 8(c)). Figure 8(b) is the same as figure 8(a) but with a different color scale, which permits visualizing details of the near field map. In the resonant case (figures 8(a) and (b)), the second FP mode does not interact with any RAs, so there are no abrupt intensity variations in its vicinity, and the enhanced transmission zone adopts a flame shape. It is evident the high intensification

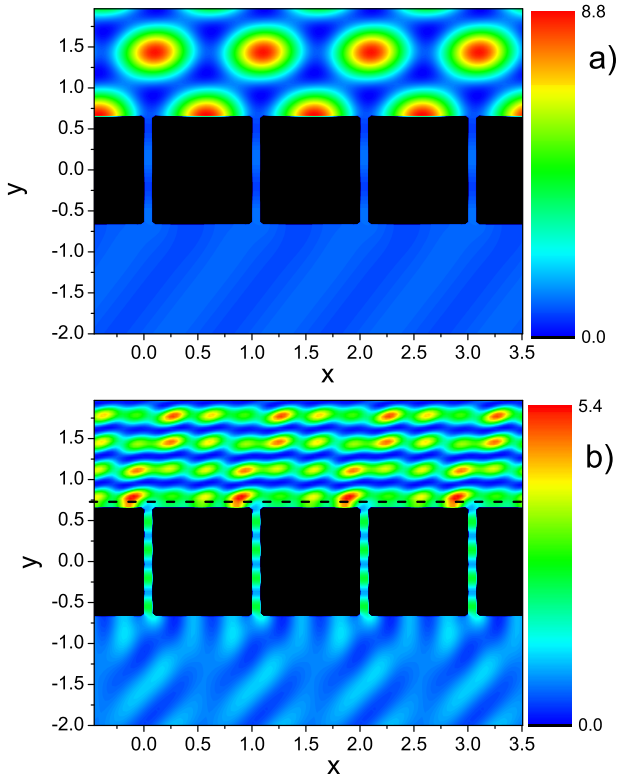

Figure 7. Near field intensity maps for the circled zones in figures 2 and 3. (a) Propagating incidence case: $\epsilon_1 = \epsilon_0$, $h/d = 1.3$, $\theta_0 = 25°$ and $\lambda/d = 1.42$; (b) evanescent incidence case: $\sqrt{\epsilon_1} = 1.5$, $h/d = 1.3$, $e/d = 0.1$, $\theta_0 = 46°$ and $\lambda/d = 0.69$.

of the electromagnetic field within the slits, which shows that it corresponds to the second FP mode. Figure 8(b) permits visualizing details in the reflected (upper zone) and transmitted (lower zone) fields. The horizontal dashed line indicates the location of the planar dielectric interface. In figure 8(c) we show the near field for a non-resonant case. A weak evanescent-to-propagating conversion is visualized, which corresponds to the -1 transmitted order (for this set of parameters the -1 order is the only contribution to the far field, see figure 5(c)).

6. Discussion and conclusions

We have investigated the influence of Rayleigh anomalies in the enhanced transmission phenomenon. In particular, we analyzed the case of evanescent-to-propagating conversion, which can be enhanced under transmission intensification conditions. We have verified that far from the occurrence of Rayleigh anomalies, the enhanced transmission regions can be very well predicted by using the infinitely thin slit approximation for the Fabry–Perot resonances. However, we have shown that RAs strongly modify this electromagnetic response, and this can be understood taking advantage of the simplified model presented. The existence of surface waves modifies the coupling condition between the fields inside and outside the slits.

The above characteristics of the enhanced transmission are also present when the incident wave is an evanescent wave. The interplay between FP resonances and RAs does not change. However, the distribution of enhanced transmission zones in the θ_0–λ/d plane is substantially modified. The intensification regions appear more confined, and this allows

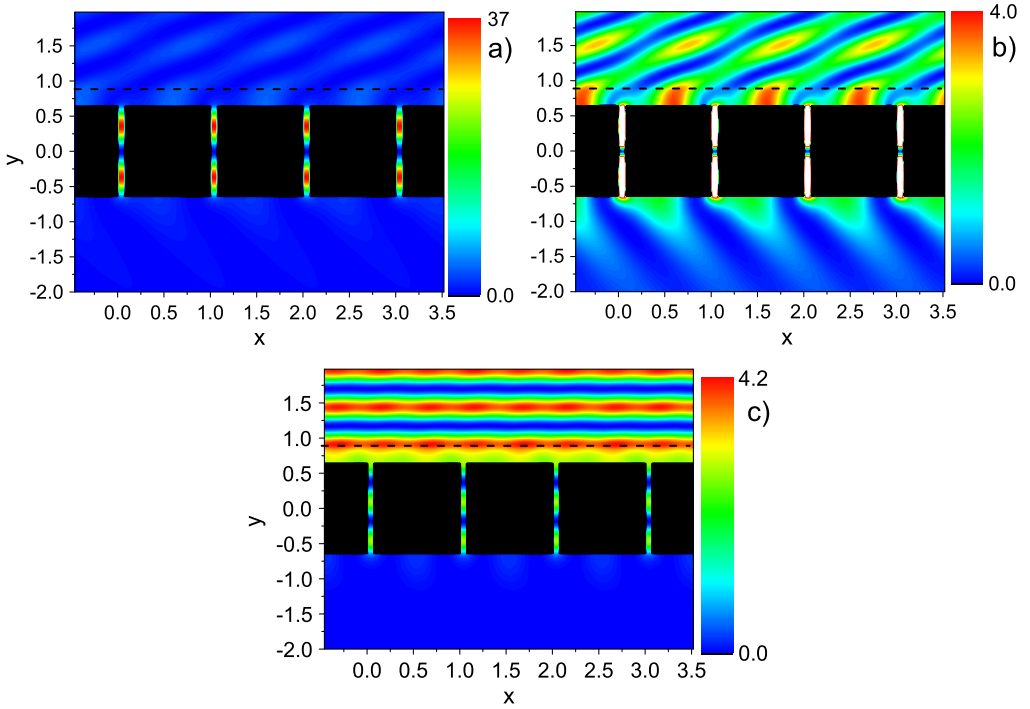

Figure 8. Near field intensity maps for the circled zones in figure 5(c). (a) and (b) resonant case: $\sqrt{\epsilon_1} = 1.5$, $h/d = 1.3$, $e/d = 0.2$, $\theta_0 = 46°$ and $\lambda/d = 1.45$; (c) non-resonant case: $\sqrt{\epsilon_1} = 1.5$, $h/d = 1.3$, $e/d = 0.2$, $\theta_0 = 46°$ and $\lambda/d = 1.1$.

to control the resonant conditions by appropriately choosing the geometrical parameters of the structure and the incidence conditions. The resonant coupling between the evanescent field and the diffraction structure strongly depends on the incidence angle and of the spacing between the array and the planar interface. Similarly to what occurs in the case of resonant surface plasmon coupling, there exist optimum values of the distance between the array and the interface which couple more efficiently the incident evanescent waves and the FP modes. The angular width of the resonances is governed by the diffraction orders. One of the most striking conclusions of this work is that even without FP resonance excitation, it is possible to have enhanced transmission due to the pseudoperiodicity of the fields. The findings reported in this work open new possibilities for the design of efficient optical devices such as tunable filters.

Acknowledgments

DS gratefully acknowledges support from CONICET (PIP 112-200801-01880) and UBACyT (20020100100533). ML gratefully acknowledges support from CONICET (PIP 0145) and Universidad Nacional del Centro de la Provincia de Buenos Aires (UNICEN).

Appendix. Expressions of the quantities involved in equations (5)

$$D_1 = \operatorname{cotan}(kh/2),$$

$$D_2 = \tan(kh/2),$$

$$V = d\left[1 + \frac{(1+K_0)}{(1-K_0)}\right] G_0 \mathcal{A}_0^+,$$

$$S = \mathrm{i}\frac{k}{d}\sum_n \frac{\mathcal{A}_n^- \mathcal{A}_n^+}{\beta_{2n}},$$

$$\Delta = (SD_1 + c)(UD_2 + c) + (UD_1 - c)(SD_2 - c),$$

$$U = d\sum_n \mathcal{A}_n^+ (1 + K_n) H_n,$$

$$K_n = \mathrm{e}^{\mathrm{i}2\beta_{2n}e}\,\frac{(-\beta_{1n} + \beta_{2n}\,\epsilon_1)}{(\beta_{1n} + \beta_{2n}\,\epsilon_1)},$$

$$G_n = 2\,\beta_{1n}\,\mathrm{e}^{\mathrm{i}\beta_{2n}e}\,\frac{1}{(\beta_{1n} + \beta_{2n}\,\epsilon_1)},$$

$$H_n = -\mathrm{i}k\frac{\mathcal{A}_n^-}{\beta_{2n}(1 - K_n)},$$

$$\mathcal{A}_n^\pm = \frac{2\,\mathrm{e}^{\pm\mathrm{i}\alpha_n c/2}}{\alpha_n}\,\sin(\alpha_n c/2),$$

References

[1] Park D J, Choi S B, Ahn K J, Kim D S, Kang J H, Park Q-H, Jeong M S and Ko D-K 2008 Experimental verification of surface plasmon amplification on a metallic transmission grating *Phys. Rev.* B **77** 115451

[2] Durant S, Liu Z, Steele J M and Zhang X 2006 Theory of the transmission properties of an optical far-field superlens for imaging beyond the diffraction limit *J. Opt. Soc. Am.* B **23** 2383–92

[3] Hao X, Kuang C, Li Y and Liu X 2013 Evanescent-wave-induced frequency shift for optical superresolution imaging *Opt. Lett.* **38** 2455–8

[4] Lee J W, Seo M A, Park D J, Jeoung S C, Park Q H, Lienau Ch and Kim D S 2006 Terahertz transparency at Fabry–Perot resonances of periodic slit arrays in a metal plate: experiment and theory *Opt. Express* **14** 12637–43

[5] Gadsdon M R, Hooper I R and Sambles J R 2008 Optical resonances on sub-wavelength silver lamellar gratings *Opt. Express* **16** 22003–28

[6] Anishur Rahman A T M, Majewski P and Vasilev K 2012 Extraordinary optical transmission: coupling of the Wood–Rayleigh anomaly and the Fabry–Perot resonance *Opt. Lett.* **37** 1742–4

[7] Kim S H, Lee C M, Park D W, Noh S K, Sim S B, Kim J, Kim G H, Ahn K J, Kim D S and Yee K J 2013 Evolution of surface plasmon resonance with slab thickness in hybrid nano-structures of Au/InGaAs slab waveguide *Appl. Phys.* B **115** 77–83

[8] Eremina E, Eremin Y, Grishina N and Wriedt T 2008 Analysis of light scattering in the evanescent waves area by a cylindrical nanohole in a noble–metal film *Opt. Commun.* **281** 3581–6

[9] Eremina E, Eremin Y, Grishina N and Wriedt T 2009 Spectral scattering properties of a nanohole in a noble–metal film in the evanescent waves area *J. Quant. Spectrosc. Radiat. Transfer* **110** 1518–25

[10] Lester M and Skigin D 2007 Coupling of evanescent s-polarized waves to the far field by waveguide modes in metallic arrays *J. Opt. A: Pure Appl. Opt.* **9** 81–7

[11] Skigin D and Lester M 2006 Study of resonant modes of a periodic metallic array near a dielectric interface: evanescent-to-propagating coupling via surface plasmon excitation *J. Opt. A: Pure Appl. Opt.* **8** 259–67

[12] Porto J A, García-Vidal F J and Pendry J B 1999 Transmission resonances on metallic gratings with very narrow slits *Phys. Rev. Lett.* **83** 2845–8

[13] García-Vidal F J, Martín-Moreno L, Moreno E, Kumar L K S and Gordon R 2006 Transmission of light through a single rectangular hole in a real metal *Phys. Rev.* B **74** 153411

[14] Skigin D C 2009 Transmission through subwavelength slit structures with a double period: a simple model for the prediction of resonances *J. Opt. A: Pure Appl. Opt.* **11** 105102

[15] Ghaemi H F, Thio T, Grupp D E, Ebbesen T W and Lezec H J 1998 Surface plasmons enhance optical transmission through subwavelength holes *Phys. Rev.* B **58** 6779–82

[16] Astilean S, Lalanne Ph and Palamaru M 2000 Light transmission through metallic channels much smaller than the wavelength *Opt. Commun.* **175** 265–73

[17] Takakura Y 2001 Optical resonance in a narrow slit in a thick metallic screen *Phys. Rev. Lett.* **86** 5601–3

[18] Gordon R and Brolo A 2005 Increased cut-off wavelength for a subwavelength hole in a real metal *Opt. Express* **13** 1933–8

[19] Gordon R 2006 Light in a subwavelength slit in a metal: propagation and reflection *Phys. Rev.* B **73** 153405

[20] Quémerais P, Barbara A, Le Perchec J and López-Ríos T 2005 Efficient excitation of cavity resonances of subwavelength metallic gratings *J. Appl. Phys.* **97** 053507

[21] Medina F, Mesa F and Skigin D C 2010 Extraordinary transmission through arrays of slits: a circuit theory model *IEEE Trans. Microw. Theory Tech.* **58** 105–15